



ELSEVIER

Spectrochimica Acta Part B 56 (2001) 2449–2464

SPECTROCHIMICA
ACTA
PART B

www.elsevier.com/locate/sab

Spectral, spatial and temporal characteristics of a millisecond pulsed glow discharge: metastable argon atom production

Glen P. Jackson^a, Cris L. Lewis^a, Stephen K. Doorn^b, Vahid Majidi^b,
Fred L. King^{a,*}

^aDepartment of Chemistry, West Virginia University, P.O. Box 6045, Morgantown, WV 26506-6045, USA

^bLos Alamos National Laboratory, Chemistry Division, CST-9, MS E518, Los Alamos, NM 87545, USA

Received 25 July 2000; accepted 18 August 2001

Abstract

Time resolved atomic emission, atomic absorbance, and laser-induced atomic fluorescence measurements of a millisecond pulsed glow discharge, made perpendicular to the insertion probe, provide temporal profiles of $1s_5$ (3P_2) and $1s_3$ (3P_0) metastable argon atom populations. Acquisition of these profiles at different spatial positions in the plasma provides data from which two-dimensional spatial plots of relative populations are constructed. Each map, the result of 368 individual pulse profiles, provides insight into the production of metastable argon atoms as a function of time and position within the plasma. During power application, intensities plateau after 3 ms as the plasma reaches a steady state condition. Metastable argon atoms are most abundant 1–2 mm above the cathode surface during this time. Excitation mechanisms such as electron excitation and fast atom/ion impact appear to dominate in this temporal regime. In contrast, argon ion–electron recombination dominates metastable formation after pulse termination. The relative population maximum for metastable argon atoms in the afterpeak shifts to 5–9 mm above the cathode surface. This shift should impact signals for analyte species generated by Penning processes in the plasma. Absorption and fluorescence measurements of the 3P_2 (11.55 eV) and the 3P_0 (11.72 eV) metastable argon atom states indicate possible differences in the populations of these two states between the plateau and afterpeak time regimes. © 2001 Elsevier Science B.V. All rights reserved.

Keywords: Pulsed glow discharge; Atomic absorbance; Atomic emission; Laser-induced atomic fluorescence; Metastable argon atoms; Two-dimensional imaging

* Corresponding author. Tel.: +1-304-293-3435; fax: +1-304-293-4904.

E-mail address: fking@wvu.edu (F.L. King).

1. Introduction

The analytical glow discharge (GD) is a valuable tool for the direct analysis of conducting and non-conducting solids.[1–3]. It is essential to understand the mechanisms of excitation and ionization in the GD in order to optimize the plasma's analytical performance. Extensive studies and modeling of excitation and ionization mechanisms appear in the literature for steady state d.c.-powered glow discharges [2,4–7]. There is markedly less information in the literature regarding these mechanisms for rf-powered and pulsed glow discharges even though these two adaptations of the glow discharge appear to hold the greatest promise for analytical applications [8].

The pulsed, or modulated, application of discharge power produces higher instantaneous concentrations of analyte ions and greater instantaneous emissions than possible with steady state d.c. current [9–13]. In such operations, the increased instantaneous power applied during the 'on' pulse improves sputter atomization and excitation/ionization; whereas, the 'off' period allows the cathode to cool and avoid overheating.

Duncen et al. [14] show that interference from residual gases reach a minimum during the afterglow time period of these plasmas. The resulting decrease in background signals coupled with high atomic ground state populations affords improved detection limits for atomic absorption [9,15,16] and atomic fluorescence [15,17–19]. Other research results demonstrate an enhancement in emission from the analyte species in the afterpeak [11,12,20,21]. Observations made perpendicular to the axis defined by the insertion probe afford an additional analytical advantage over 'end-on' measurements because spatial variations of plasma processes can be exploited [19,22,23].

The mechanisms responsible for afterpeak emission by the sputtered analyte species are more complex than a capture-cascade model would predict [24,25]. For instance, emission often occurs for a time that is several orders of magnitude longer than the lifetimes of the excited states. This observation strongly suggests a role for long-lived species such as metastable argon

atoms. Indeed, Strauss et al. [20] demonstrate that metastable argon atoms play a significant role in the excitation of copper atoms in the afterpeak (at ~ 1.8 torr, 40 mA, 400 V). Although the exact mechanism of energy transfer is uncertain, in the absence of Cu II emissions, they rule out the possibility of Penning ionization. This analysis overlooks the fact that the residual energy from Penning ionization is insufficient to populate excited states of the copper ion, thus the lack of emission alone cannot rule out the role of Penning ionization. A possible mechanism would be Penning ionization of sputtered analyte atoms followed by electron-ion recombination, leading to radiative relaxation.

In fact, mass spectrometric sampling of these plasmas demonstrates that analyte ion formation is enhanced after power termination [11,26–28]. It appears that these analyte ions form in the afterpeak via Penning ionization. Observations that (1) the argon ion concentration diminishes before the analyte ion afterpeak maximizes; and (2) analyte ion densities exceed those of argon ions support this conclusion [29]. The addition of methane to the discharge gas [30,31] to quench metastable argon atoms also inhibits ionization of sputtered species in the afterpeak, again strongly implying a role for Penning ionization [26,27]. Following this line, Majidi and co-workers observe distinct differences in ionization mechanisms between the steady state conditions and the afterpeak when they introduce organic vapors into pulsed glow discharges [32,33]. In those investigations they observe different fragmentation patterns for organics during different time periods in the pulse cycle. The fragmentation patterns observed in the afterpeak strongly suggest reactions with species having energy equivalent to that of metastable argon atoms.

In steady state GDs, it has long been considered that metastable discharge gas atoms play an important role in the ionization of sputtered species [34]. Hess and co-workers [35,36] show that Penning ionization is responsible for 40–80% of the ionization of sputtered species in argon glow discharges operating at 0.5–1.2 torr, 1–5 mA, and 500–3500 V. If Penning ionization accounts for 40–80% of ionization during voltage

application, one might expect that this percentage would be larger in the afterpeak time regime where fewer competing ionization mechanisms are possible.

Because metastable argon atoms are so important in the pulsed GD plasma, this paper focuses on the investigation of these species. In this study laser induced atomic fluorescence (LIF), atomic emission, and atomic absorption measurements provide insight into the formation and disappearance of the two metastable argon atom states (3P_2 state at 11.55 eV and 3P_0 state at 11.72 eV). This study should provide a better understanding of the spatial and temporal dynamics occurring within the discharge gas. Our investigations of other species such as analyte atoms/ions, argon ion species, and non-metastable excited state argon atoms are ongoing and will appear separately.

2. Experimental

Fig. 1a shows the optical setup used for emission and absorption experiments. A stainless steel six-way cross (MDC, MFG Inc., Hayward, CA) with Suprasil optical view ports (Heraeus Quartz, Duluth, GA) housed the glow discharge source. The 4-mm diameter copper disk samples (unalloyed copper NIST SRM 495, Gaithersburg, MD) were introduced via a 1.27-cm ball valve using a direct insertion probe. Ultra pure Argon (Airgas, Radnor, PA) at 0.8 torr was used as the discharge gas. Supporting the discharge was a fast-response power supply (Kepco OPS-3500, Flushing, NY), modulated using a pulse generator constructed in-house. Pulse width and frequency were maintained at 5.0 ms and 50 Hz respectively, giving a duty cycle of 25%. The applied voltage was measured using a high voltage probe (Tektronix P6015, Beaverton, NY) with 1 M Ω , 20 pF termination to an oscilloscope (Tektronix 2232, Beaverton, NY). The current was measured using a current meter in line with the power supply. The pressure was determined with a thermocouple vacuum gauge (Teledyne Hastings, Hampton, VA).

2.1. Emission experiments

For optical emission experiments two plano-

convex lenses imaged the light in a 1:1 ratio onto the entrance slit of a 0.64-m monochromator (ISA HR-640, Edison, NJ). Entrance and exit slits were 50- μ m wide and 1-mm high throughout the study. The radiation was dispersed on a 1200-groove mm⁻¹ holographic grating and detected using an extended-red photomultiplier tube (Hamamatsu R-928, Bridgewater, NJ). The output was monitored by an oscilloscope (Lecroy 9370M, Chestnut Ridge, NY) with 1-M Ω termination. Software (Lecroy Scope Explorer) was used to transform the data into ASCII format.

2.2. Absorbance measurements

For absorbance measurements, a mechanical chopper (EG & G197, Princeton, NJ) modulated the incident beam from the hollow cathode lamp (Beckman Cu–Ne HCL for Cu lines and B–Ar for Ar lines). The hollow cathode lamps (HCLs) were operated at 15 mA constant current using a d.c. power supply (Kepco BHK-2000, Flushing, NY). The incident beams were focussed midway through the plasma before collection using the same system described for emission experiments. The signal from the PMT was measured with a lock-in amplifier (LIA) (EG & G PAR 5210, Princeton, NJ) tuned to the chopper frequency of 3 kHz. The output from the LIA was monitored on the oscilloscope (with 50 Ω termination). The smallest time-constant of 1 ms was utilized to obtain the fastest response time. Because the RC time constant caused distortion of the absorption temporal profiles, a program was written in MICROSOFT EXCEL VISUAL BASIC to deconvolute the data. The deconvolution process is described in Appendix A. At each position within the plasma 2500 data points were collected over a 20-ms time period, and were smoothed twice with a moving average of 10 data points.

The six-way cross housing the GD was mounted on an adjustable support such that the housing could be moved orthogonally with respect to the monochromator axis. To vary the height above the cathode, the insertion probe was carefully maneuvered up and down. In this way, the optics remained constant throughout data acquisition to reduce the risk of skewed results. Data were

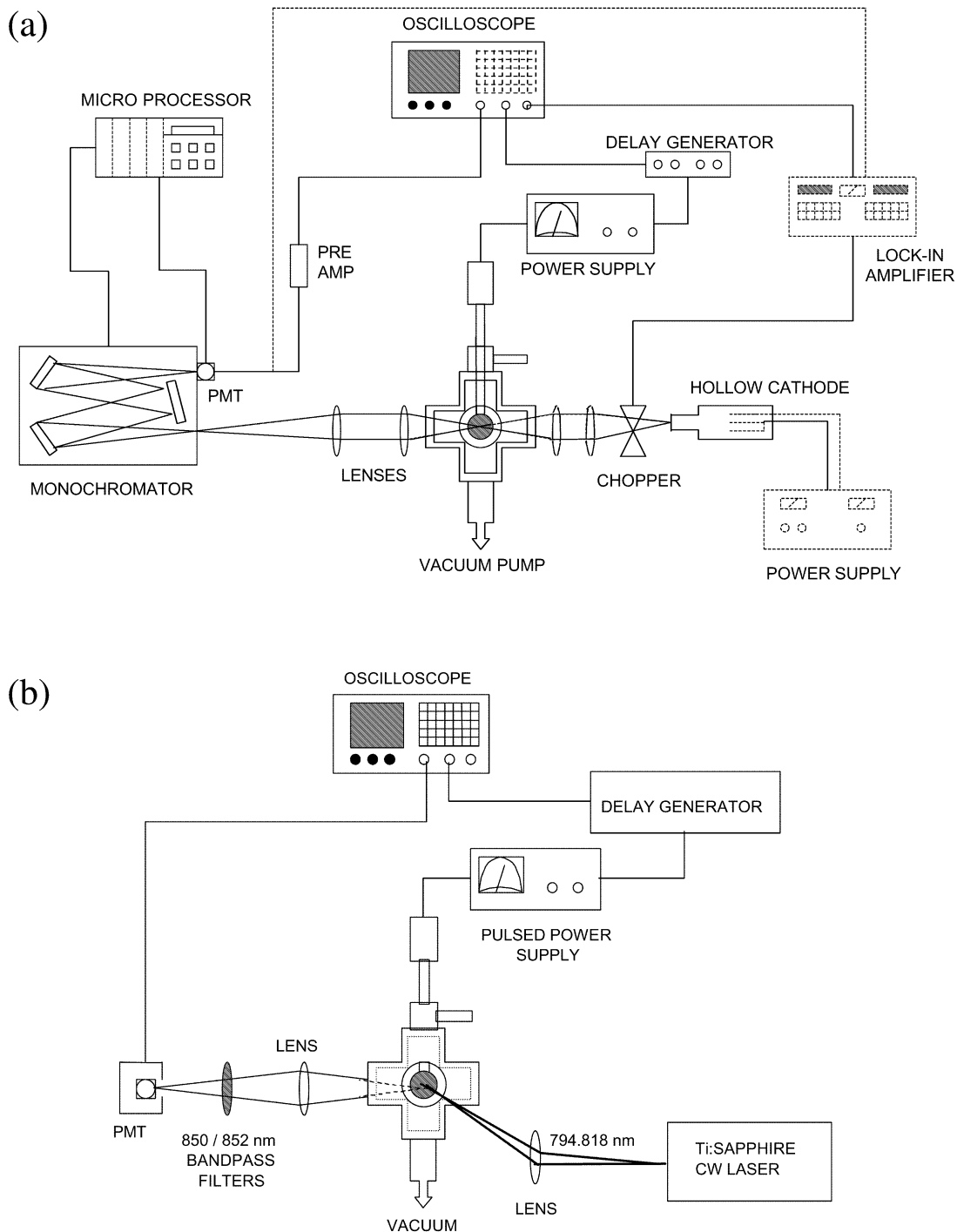


Fig. 1. Schematic diagram of (a) the orthogonal glow discharge system used for emission and absorbance measurements; and (b) the system used for laser induced fluorescence.

collected at 368 spatial positions for each map, up to 18 mm vertically and 8 mm horizontally [43]. Resolution is lower at positions that are far from the cathode where it is assumed that dramatic changes in populations do not occur. A program was written in MICROSOFT EXCEL VISUAL BASIC to process the large number of data files used for each map. The maps generated with the program were manually verified to ensure that the data had been transferred correctly.

2.3. Laser induced atomic fluorescence

For LIF experiments a different experimental setup was utilized (see Fig. 1b). The glow discharge chamber was a six-way, high vacuum, stainless steel cross (MDC, Hayward, CA). Three side ports on the cross were fitted with optical view ports (Heraeus Suprasil Quartz, Duluth, GA). The fourth side port was used as both a gas inlet and vacuum. A Pirani pressure gauge was used for pressure monitoring. The top port is used for introduction of the cathode direct insertion probe. The cathode was a 6-mm diameter, 1-mm-thick copper disk attached to the probe using silver paint, and isolated from the probe sides using a concentric Macor cylinder. The chamber mount allowed for vertical and side-to-side translation (along the axis of the laser excitation beam).

The discharge pulse was triggered as follows: a delay generator (Stanford Research Systems DG535, Palo Alto, CA) defined the discharge pulse duration. A 5.0-ms output pulse from the delay generator triggered the glow discharge high voltage power supply (Kepco OPS-3500, Flushing, NY). The resultant 5.0-ms glow discharge pulse was operated at 50 Hz and approximately 1 kV.

The metastable argon atom $1s_3-2p_4$ transition (see Fig. 2) was excited using an Ar ion laser pumped titanium sapphire laser (Spectra Physics 3900) tuned to 794.818 nm with a bandwidth of 1 cm^{-1} , which at 794.818 nm translates to 0.064 nm. The incident light (75 mW) was focused into the discharge cell with a 250-mm focal length planoconvex lens, and was aligned to pass directly beneath the center of the glow discharge cathode. Laser induced fluorescence from the $2p_4-1s_2$

transition at 852.144 nm was collected at 90° with respect to excitation by a 50-mm diameter, 250-mm focal length biconvex lens. The lens was positioned equidistant between the cathode and detector for one-to-one imaging of the discharge. Collected light passed through two narrow bandpass filters (850 nm by 10 nm bandpass, and 852 nm by 5 nm bandpass) used for rejection of the plasma background emission. The collected light was imaged on a 1-mm pinhole (to provide a spatial mask) and is detected by a PMT (R955, Hamamatsu Corp.) located directly behind the pinhole. The PMT signal response was confirmed to be linear over the range of signal intensities observed.

Output from the PMT was acquired with a digital storage oscilloscope (Tektronix TDS 520C, Beaverton, OR) using a $1\text{-M}\Omega$ input impedance and $4\text{-}\mu\text{s}$ per point timebase resolution. The scope was triggered synchronously with the discharge using the delay generator. An average of 256 traces were acquired at each plasma position and transferred to a PC for further analysis. Even with the use of two rejection filters in the collection path, significant plasma background was observed in the wavelength region of the fluorescence signal. Emission traces were obtained at each plasma position with and without laser excitation for background subtraction. Data were obtained at the same spatial positions as described for the emission and absorption experiments. Whereas the absorption and emission data were collected in horizontal slices, LIF data were collected in vertical slices by moving the direct insertion probe before moving the housing to the next horizontal position. At the end of each vertical slice the plasma was returned to the (0,0) position to measure the extent of drift. Each vertical dimension could then be normalized to account for any drift in incident laser wavelength (which resulted in a drop in LIF intensity).

3. Results and discussion

This study considers the two metastable argon atom states — $(1s_5) \ ^3P_2$ at 11.55 eV and $(1s_3) \ ^3P_0$ at 11.72 eV — separately because of their dif-

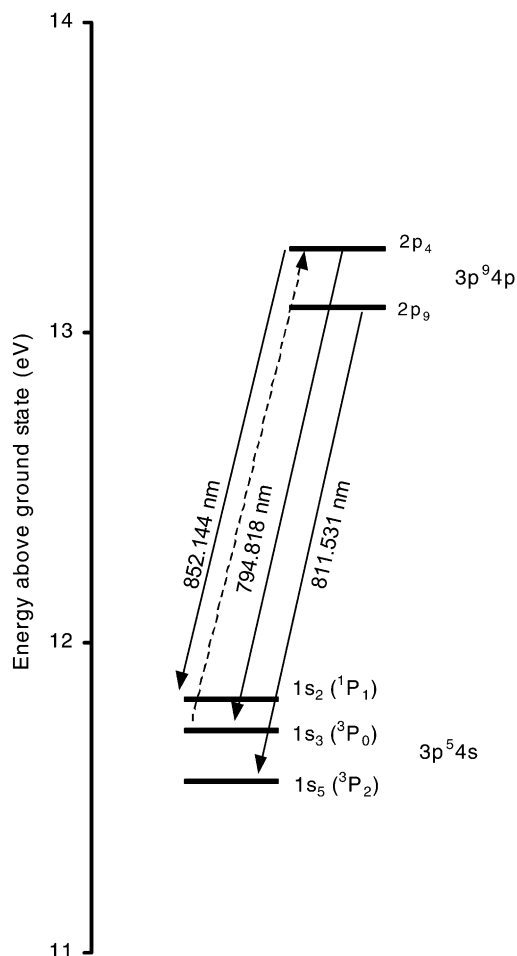


Fig. 2. Energy level scheme and transitions, relevant to this experiment, for the argon atom metastable states of 3P_2 (11.55 eV) and 3P_0 (11.72 eV).

ferent formation and quenching rates [31,37–40]. Fig. 2 shows a simplified energy level scheme of the transitions used to monitor the two metastable states. Absorbance and emission measurements were made of both the 794.8- and 811.5-nm lines along with laser pumping at 794.8 nm followed by emission at 852.1 nm.

Fig. 3a shows a typical applied voltage pulse as used for the absorption and emission experiments (the applied voltage for the LIF experiments was essentially a square wave, having a fall time $< 8 \mu\text{s}$, and is not presented). Because the rise time is approximately 1 ms, a 5.0-ms pulse width ensures

that steady state conditions are reached. The fast fall time aids in the formation of an afterpeak [28] and helps eliminate processes, such as electron excitation, that could be stimulated by the presence of an electric field.

Fig. 3b shows a typical temporal absorption profile taken 5.0 mm above the center of the cathode, before deconvolution, for the 811.5-nm transition. The effects of the 1-ms time constant in the LIA are evident in that the profile never reaches a plateau and the afterpeak is delayed and broadened. Deconvolution of the data (see Appendix A) yields the trace shown in Fig. 3c. In this case, steady state conditions appear shortly after 2 ms, the afterpeak is more apparent, and the afterpeak shifts to a shorter time of 5.7 ms. The absorption plot shown clearly indicates an increase in the metastable argon atom population during the afterpeak time regime.

The emission at 811.5 nm (Fig. 3d), also taken at 5 mm, corresponds to the argon atom transition from $2p_4-1s_5$, 13.08–11.55 eV, and represents the highest transition probability for formation of the 3P_2 metastable. Shortly after pulse termination, a noticeable afterpeak appears at 5.35 ms, just before the maximum in the absorbance value. This observation is consistent with

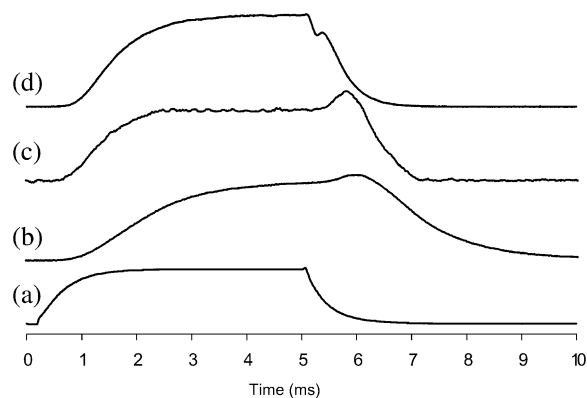


Fig. 3. Temporal profiles showing (a) the applied voltage; (b) raw absorbance data at 811.5 nm before deconvolution; and (c) the same data after deconvolution and smoothing twice with a moving average of 10 points; and (d) emission profile for 811.5 nm. Conditions; 5 ms pulse, 25% duty cycle (50 Hz), 0.8 torr, 1.8 mA peak current, 860 V peak voltage (~ 1.5 W peak power), 5 mm above cathode center.

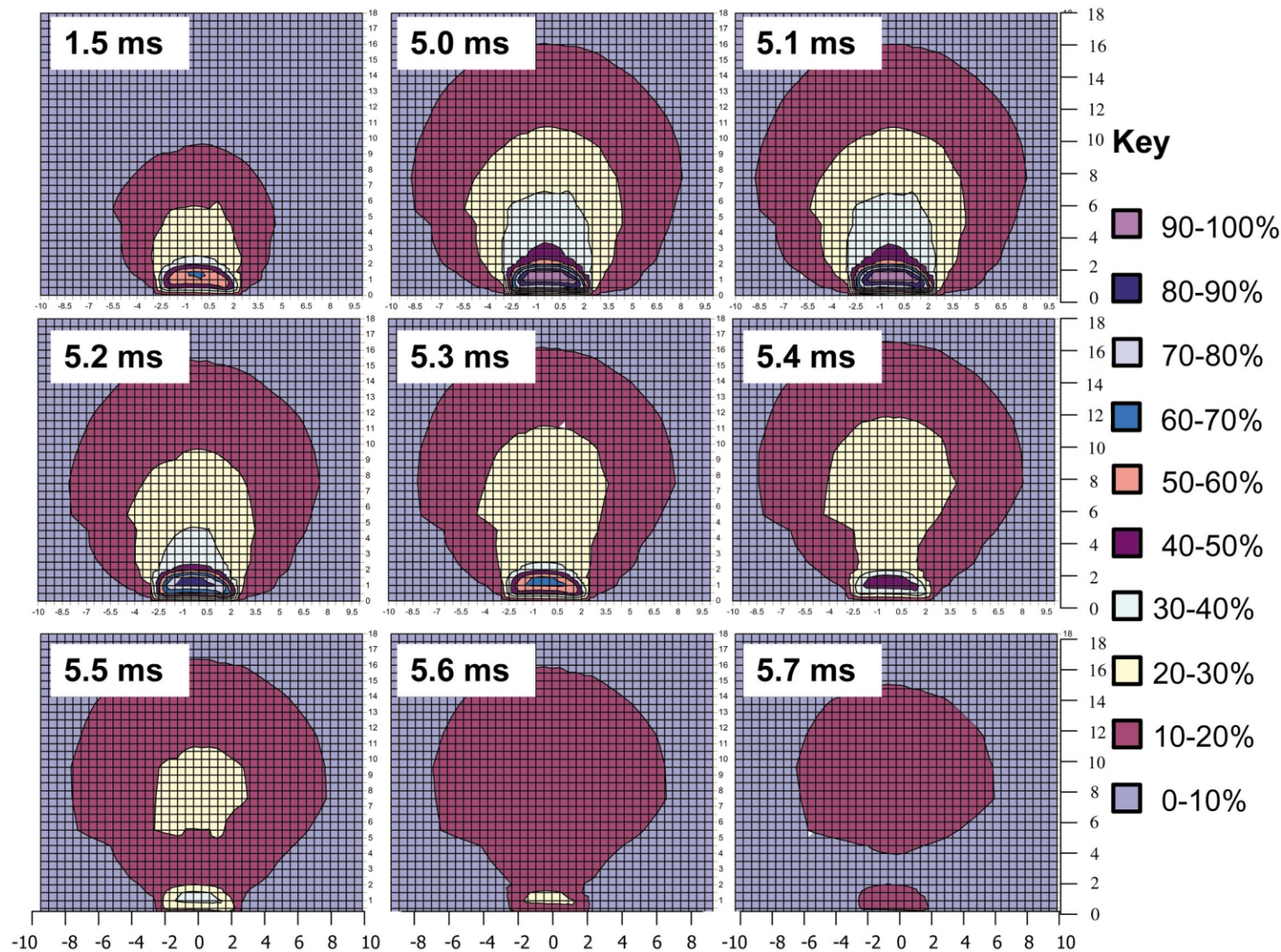


Fig. 4. Two-dimensional images of argon atom emission at 811.5 nm. Conditions; 5-ms pulse, 25% duty cycle (50 Hz), 0.8 torr, 1.8 mA peak current, 860 V peak voltage (~ 1.5 W peak power).

the formation of metastable argon atoms via radiative decay.

3.1.1. 3P_2 argon atom metastable: population via radiative decay

Fig. 4 shows how the emission intensity for the 811.5-nm line varies as a function of time from 1.5 to 5.7 ms. This emission corresponds to the 13.08–11.55 eV, $2p_0-1s_5$ ($^3D_3-^3P_2$) transition and exhibits the strongest emission for a transition resulting in the population of the 3P_2 metastable level. At 1.5 ms, the plasma is still forming and the emission intensity is still increasing. From 2.0 to 5.0 ms, steady state conditions are established and the emission characteristics do not change. During this steady state condition, emission intensity is low immediately at the cathode and increases rapidly to a maximum 1.0–1.5 mm above the surface. The intensity decreases rapidly from 1.5 to 2.5 mm but decreases more slowly at distances greater than 2.5 mm. This behavior is similar to observations made by Hoppstock and Harrison for a glow discharge operating under steady state conditions [41]. The intense emission focussed ~ 1 mm defines the negative glow directly adjacent to the cathode dark space. In steady state discharges, the 4p states are in a high state of flux and are thought to be populated in almost equivalent amounts by electron excitation from the ground state, electron excitation from a 4s state and by radiative decay from higher levels [42]. Significant depopulation processes include radiative decay to 4s levels (as observed by the 811.5-nm emission in this case) and electron excitation to higher levels. Notice that the 4s levels and highly excited states thus formed are capable of repopulating the 4p levels.

Upon power termination the emission intensity within 4 mm of the cathode simply decreases and shows no post-pulse enhancement. The region positioned 6 mm above the cathode remains almost constant between 5.0 and 5.5 ms. The area between 7 and 8 mm can be seen to decrease in intensity between 5.0 and 5.3 ms, but then increase through 5.4–5.5 ms. Because the emission intensity actually increases, the 4p population processes must be enhanced in this vicinity from 5.3 to 5.5 ms. This leads us to propose a method

of populating the ~ 13 eV levels in the absence of a strong electric field. Because there are no strong coulombic forces with which to accelerate unbound electrons, electron excitation can be ruled out (for the same reason, depopulation of the $2p_0$ state via electron excitation to higher levels is also reduced). The significant mechanisms remaining with which to feed this state are radiative decay and collisional deexcitation from higher excited states. The highly excited states are also unable to be populated by electron excitation, however, so must be populated via electron-ion recombination. The main process leading to the observed increase of emissions at 811.5 nm in the afterpeak is expected to commence with both radiative and collisional recombinations of argon ions (formed during power application) and thermal electrons.

3.1.2. 3P_2 argon atom metastable: absorption

The absorbance at 811.5 nm accompanies the transition from the (3P_2) $1s_5$ metastable state to the $2p_0$ state. The population fluctuations in time are shown in two-dimensional maps in Fig. 5. During steady state conditions this metastable argon atom state is most abundant 1 mm above the cathode — in agreement with the emission data. After pulse termination the distribution of metastable argon atoms changes dramatically, and is similar to that observed in the emission profile, although the absorbance times are delayed. From 5.0 to 5.6 ms the metastable population hardly changes throughout the plasma. After this time, the bulk population can be seen to move away from the cathode. This movement coincides with the formation trends observed in the 811.5-nm emission maps. Close inspection of the 5.9-ms map in the region 4–8 mm away from the cathode reveals how the density of metastable argon atoms actually increases by approximately 20% compared to the steady state conditions. Klingler et al. [28] did not observe an increase in the afterpeak absorbance for the same transition under similar conditions. However, they did not give a specific distance at which they monitored the absorbance of this metastable. It is possible that their measurements were made in the beginning of the negative glow (2–3 mm from the cathode

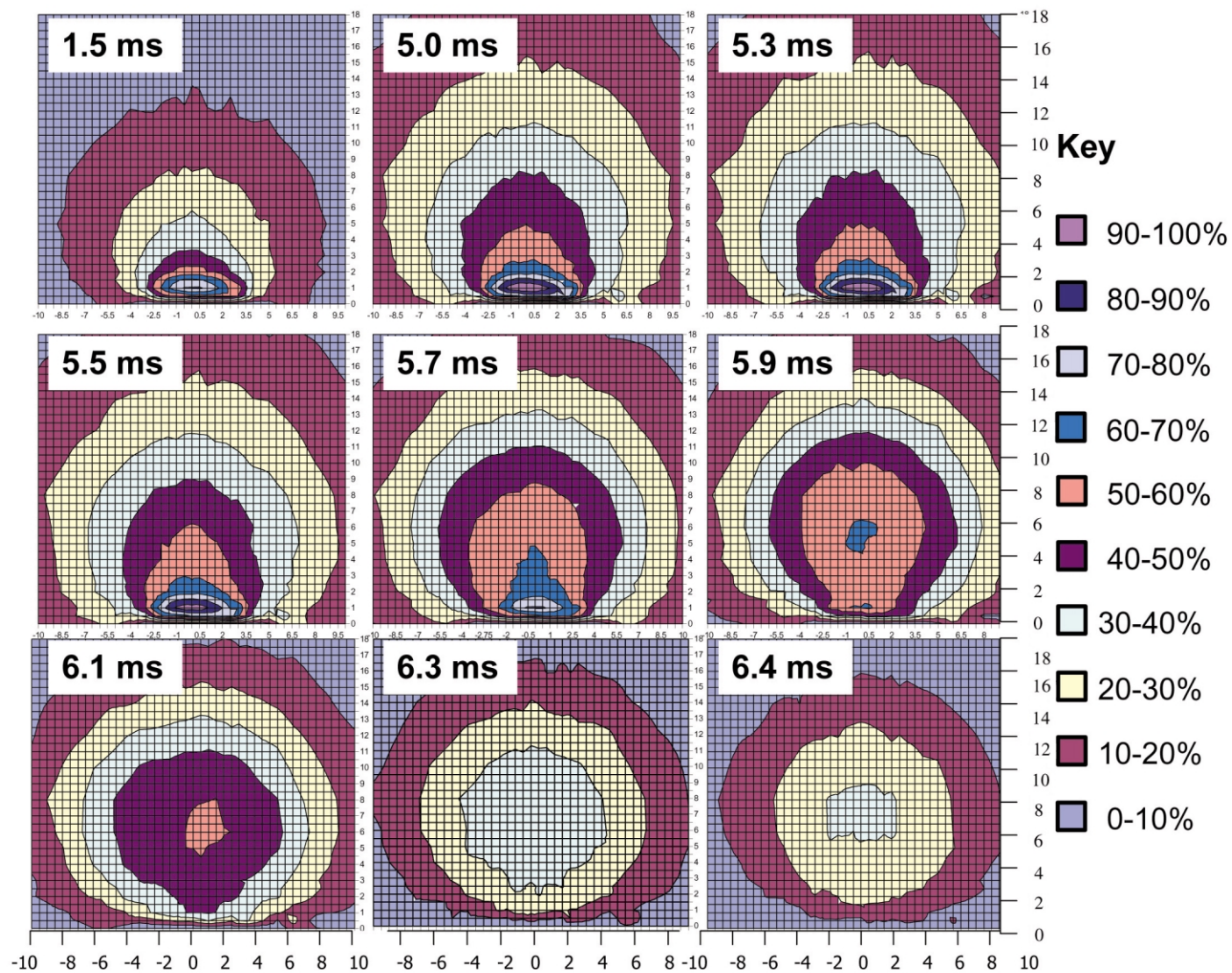


Fig. 5. Two-dimensional images of argon atom absorption at 811.5 nm. Conditions; 5 ms pulse, 25% duty cycle (50 Hz), 0.8 torr, 1.8 mA peak current, 860 V peak voltage (~ 1.5 W peak power).

surface) where there is no increase in number density in the afterpeak compared to the plateau. The maximum abundance after 5.9 ms is found between 5 and 8 mm. At 9 mm above the cathode surface, the metastable density 1.4 ms after pulse termination is within 10% of the density during the plateau. In contrast, the density 1 mm above the cathode decreases by almost 70% over the same time period.

It should be remembered that the temporal accuracy of the absorbance data is somewhat suspect because of the RC time constant effect discussed above. Deconvolution helped remove some of the time lag but it is considered that the time domain can be used more as a relative index rather than absolute for these measurements. Nonetheless, the overall trends, however, clearly indicate that the metastable argon atom distribution in the afterglow is very different from that of steady state conditions and that the population maximum is found 4–7 mm further away from the cathode surface than during steady state conditions. It is not surprising that processes dependent on this metastable state, such as Penning ionization of analyte species, would also reflect this shift [43].

3.2. 3P_0 argon atom metastable: population via radiative decay

The emission at 794.8 nm (Fig. 6), corresponds with the transition from $2p_4$ to $1s_3$, 13.28–11.72 eV. Again, intensities are normalized to the largest intensity over the entire pulse cycle. During steady state conditions (i.e. from 3 to 5 ms) the spatial emission distribution is almost identical to that of the 811.5-nm emission, although the absolute emission intensity is obviously lower (the 3P_0 level has a degeneracy of 1, while the 3P_2 level has a degeneracy of 5, and the transition probability is lower for the former: 0.186×10^8 vs. $0.331 \times 10^8 \text{ s}^{-1}$ [44]). After pulse termination at 5.0 ms, the emission intensity decays in a fashion similar to the 811.5-nm line: within 4 mm the emission intensity steadily declines, between 6 and 8 mm the intensity initially decreases before increasing, and the plasma beyond 9 mm remains relatively constant. Not accounting for metastable

loss processes, one would expect the emission maps of Fig. 6 to precede the 3P_0 population in the afterpeak.

3.3. 3P_0 argon atom metastable: absorbance and laser induced fluorescence

A spatial map for the absorbance at 794.8 nm and 4.0 ms appears in Fig. 7a. The absorption was found to be in a steady-state at this time. A spatial map for the LIF of this metastable state at 4.0 ms appears in Fig. 7b. In both maps the data have been normalized to the largest value in their respective pulse cycles. The spatial similarities between the two maps are indicative of the reproducibility of this experiment on two entirely different systems. In both cases the maximum population is found approximately 1.0 mm above the cathode, in agreement with the emission map (at 794.8 nm) and previous work by Bogaerts et al. on this species under steady-state conditions [6]. The slightly less symmetrical appearance of the LIF map may arise from incomplete intensity correction to compensate for the drift in wavelength of the excitation laser (see Section 2).

In contrast to Bogaerts et al. — who observed a second population of this metastable state further from the cathode — a second population under steady state conditions is not visible in these experiments. This could be because the cell geometry and operating conditions used in the present study differ from those that Bogaerts et al. examined. It is interesting to note that in this present study the maximum emission, absorbance and LIF values for both metastable levels appear at a distance where Ferreira et al. find the metastable populations to reach a minimum [23]. Ferreira et al. find absorbance maxima at the cathode surface and approximately 3 mm above the surface. The operating pressure had a dramatic effect on the spatial position and density of the 3P_2 metastable atom. Bogaerts et al. [6] noted that populations did not shift in space as a function of pressure and that the maxima were observed at approximately 4.0 and 12 mm. Again, such contrasting results reinforce the fact that no single descriptive model accurately addresses the

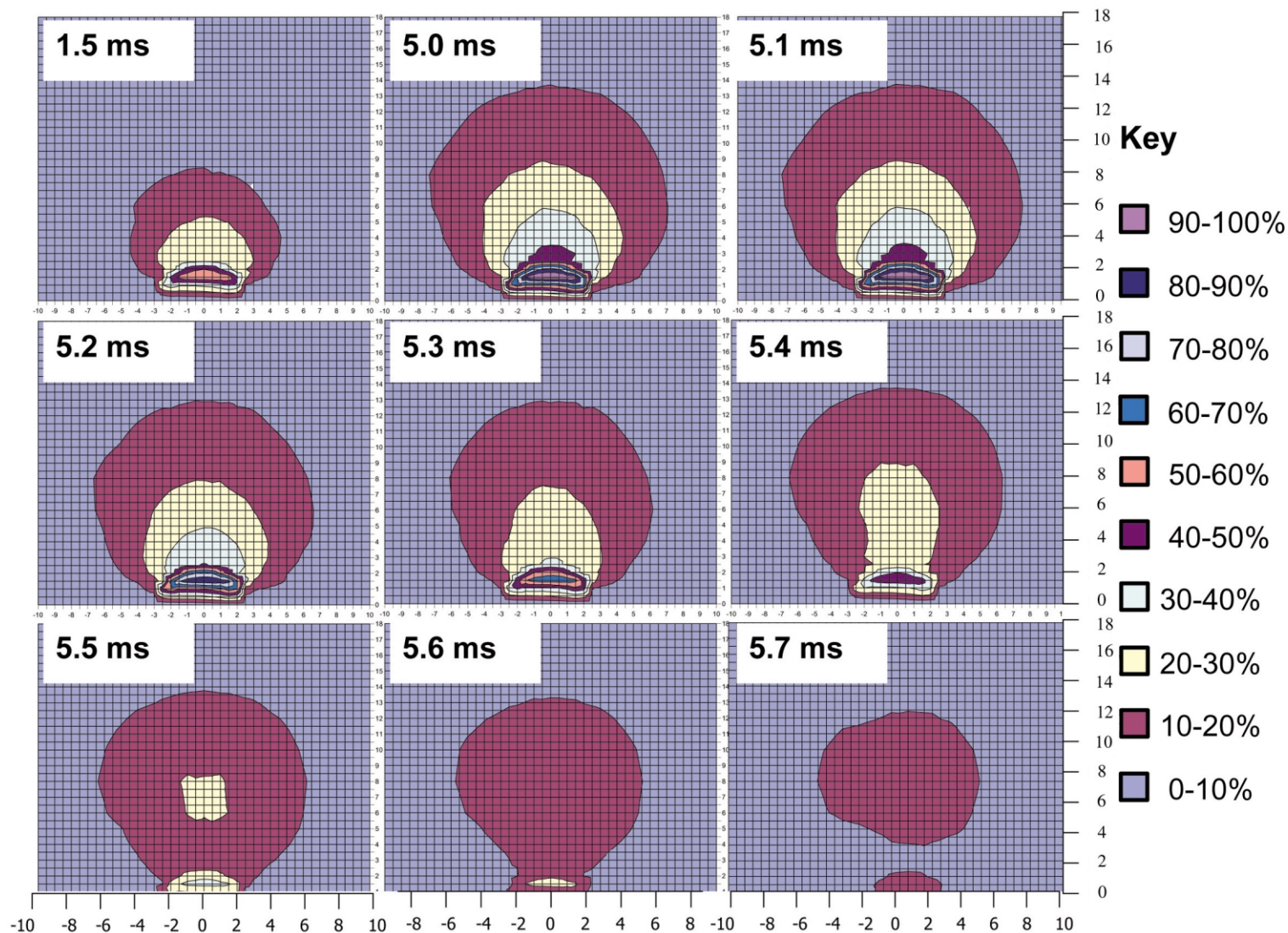


Fig. 6. Two-dimensional images of argon atom emission at 794.8 nm. Conditions; 5-ms pulse, 25% duty cycle (50 Hz), 0.8 torr, 1.8 mA peak current, 860 V peak voltage (~ 1.5 W peak power).

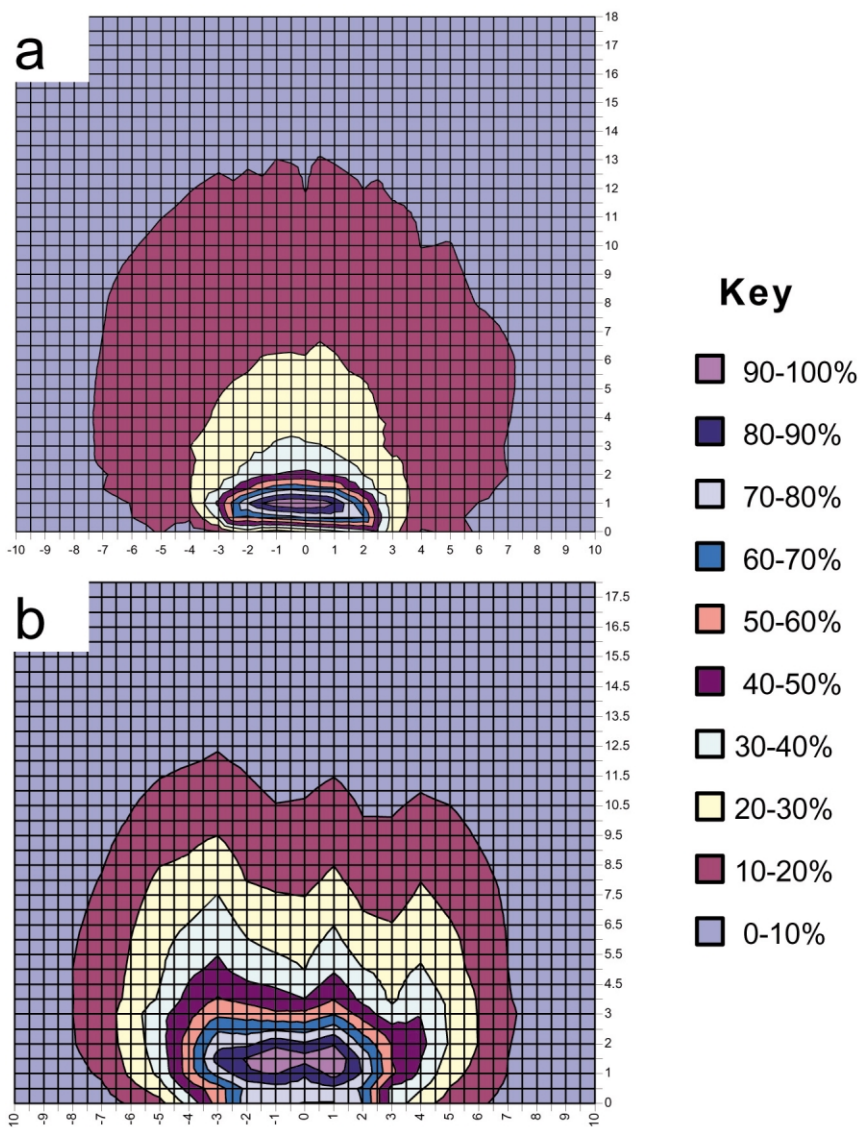


Fig. 7. Two-dimensional images of the 3P_0 metastable argon atom state at 4.0 ms by (a) absorption at 794.8 nm; and (b) laser induced fluorescence (see Section 2).

different operating conditions and cell geometries of GD sources.

In the afterpeak the population of the 3P_0 metastable state — as measured by absorbance and LIF — displays a smaller post-pulse increase than is seen for the absorption at 811.5 nm for the 3P_2 state (reasoning is provided at the end of this section). When viewed in the two-dimen-

sional map form, therefore, LIF and absorption data do not show such a significant shift in the 3P_0 state between the plateau and afterpeak time regimes. If, however, the ratio of afterpeak/plateau values are plotted as a function of distance from the cathode (Fig. 8) it is evident that the 3P_0 state is enhanced in certain areas of the afterpeak plasma. The absorbance afterpeak/

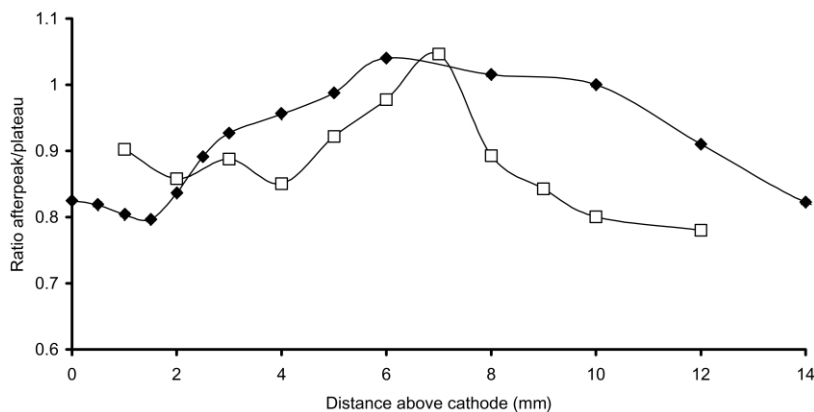


Fig. 8. Ratio of afterpeak/plateau values for the 3P_0 metastable argon atom state by \square absorption at 794.8 nm (5.5 ms/4.0 ms) and \blacklozenge laser induced fluorescence (~ 5.15 ms/4.0 ms).

plateau ratio at 7 mm is greater than 1 and implies that the number density is greater in the afterpeak than the plateau. The LIF afterpeak/plateau ratios maximize in approximately the same region (6 mm above the cathode) and again identify the post pulse increase in population of this species. The slight difference in the afterpeak/plateau maxima positions between the LIF and absorbance data is probably due to the difference in fall time of the applied pulse. As mentioned in the experimental, the fall times in the LIF and absorbance experiments are ~ 8 and ~ 800 μ s, respectively. The difference in voltage fall times is also attributed to the faster appearance of an afterpeak in the LIF experiments. The afterpeak was found to maximize ~ 200 μ s after pulse termination in the LIF study but ~ 400 μ s in the emission study.

Both absorbance and LIF measurements show smaller afterpeak/plateau ratio values close to the cathode. This reflects the lack of 3P_0 state formation and/or greater loss mechanisms in this spatial region for the afterpeak. This same phenomenon was observed for the 3P_2 state. An enhanced loss mechanism specific to this proximity is likely to be diffusion to and deexcitation at the cathode surface.

The afterpeak increase of the 3P_0 state in absorption measurements is less easily defined than that of the 3P_2 state, in these experiments. Unless the weaker afterpeak for the 3P_0 state is due to

some unforeseen experimental error, the ratio of the $^3P_2/^3P_0$ metastable levels differs quite considerably between the plateau and afterpeak time regimes. (A reviewer has pointed out that a change in the relative magnitudes of the metastable states is consistent with the reported literature on switching from an ionizing plasma to a recombining plasma. This phenomenon is discussed in detail in a follow-up paper currently in preparation.) It is safe to assume that electron-ion recombination (two or three body) followed by radiative decay is the dominant gain mechanism for both levels in the afterpeak. The 3P_2 state could therefore be more highly populated in the afterpeak if the sum of the radiative transition probabilities to the 3P_2 state exceed those to the 3P_0 state. An approximation for this calculation uses the transition probabilities and degeneracies of the 15 strongest lines leading to the formation of each metastable. The result indicates that the 3P_2 state is more probably populated than 3P_0 state by approximately one order of magnitude. The population processes for the two metastable species in the steady-state and afterpeak times are therefore different enough that the 3P_2 contributes a larger proportion of the total metastable argon atom population in the afterpeak. This finding is significant if mathematical models such as those proposed by Bogeaerts et al. [6] are based on measurements on the less-abundant 3P_0 state.

4. Conclusions

During steady state and plateau conditions the populations of both 3P_2 and 3P_0 argon atom states maximize 1–2 mm above the cathode surface. This is in general agreement with other investigations of these species in analytical glow discharges operating under similar conditions. Population processes are likely to be electron impact and fast atom/ion impact at this distance. In the afterglow, the bulk of both the 3P_2 and 3P_0 metastable states are formed 4–7 mm further from the cathode surface than during the plateau. Argon ion–electron recombination followed by radiative relaxation is the most probable mechanism of populating these levels. Ongoing work in our lab indicates that excitation and ionization of sputtered species in the afterglow is extremely dependant on these metastable argon atoms. Finally, this study has shown that the observation time and position both dramatically affect the behavior observed for species in pulsed GD plasmas.

Acknowledgements

The authors wish to thank Andy Shreve (LANL, B-S2) for the use of the Ti:sapphire laser. The WVU researchers gratefully acknowledge the support of this work by the U.S. Department of Energy, DE-FG02-00ER45837. LIF experiments were supported by LANL through the ADAPT program under the auspices of the U.S. Department of Energy. We are also grateful to Dr H.O. Finklea, Demitri Brevnov and Maria-Rosa Valero-Aracama for their assistance with the deconvolution process.

Appendix A

A.1. Theory

The deconvolution process is based on a procedure described by Jansson [45]. The smallest RC time constant of 1 ms was selected when collecting absorbance data with the lock-in amplifier.

This time constant is on the order of the pulse profiles used in this study and has the effect of distorting the input signal voltage according to the equation

$$v_c(t) = \xi(t) \otimes v(t)$$

[assuming a first order (linear) approximation of the RC time constant] where $v_c(t)$ is the output signal voltage, $v(t)$ is the input voltage and $\xi(t)$ is given by

$$\xi(t) = (1/RC)H(t)\exp(-t/RC)$$

where RC is the time constant (1×10^{-3} s), $H(t)$ is the heavy side step function, and t is the time. This can also be written in the form

$$V_c(\omega) = \Xi(\omega)V(\omega)$$

where $V_c(\omega)$ and $V(\omega)$ are the frequency spectra of the output and input voltages, respectively, and the complex filter transfer function is given by

$$\Xi(\omega) = 1/(2\pi)^{1/2}(1 - j\omega RC)/(1 + \omega RC)^2$$

A.2. Application of theory

The time axis is first modified with the heavy side step function ($t_i = \exp -t_i/RC$). Next, fast Fourier transforms (FFTs) of 2^n (i.e. 2048, or 4096) data points were performed on both the modified time axis [$H(t)$] and the digitized voltage output [$G(t)$]. An inverse FFT was performed on the quotient $\Xi[H(t)]/\Xi[G(t)]$ to obtain the deconvoluted data [$v(t)$]. After baseline correction the deconvoluted data were averaged twice with a moving average of 10 data points before being exported to a database.

As with any Fourier analysis, it was found that using a larger number of data points enhanced the deconvolution process. Unfortunately, with our current FFT software (Microsoft Excel), we are restricted to 4096 data points. A program was written in MICROSOFT VISUAL BASIC in order to deal with the huge number of data files. Each ASCII file was imported individually into a tem-

plate. After the above mathematical analysis, the deconvoluted data were transferred to a database file before importing the next raw data file. Because of the nature of the database, intensity values can be extracted to generate a 2D map for any given moment in time (to within 4 μ s).

References

- [1] R.K. Marcus, *Glow Discharge Spectroscopies*, Plenum Press, NY, 1993.
- [2] A. Bogaerts, R. Gijbels, Fundamental aspects and applications of glow discharge spectrometric techniques, *Spectrochim. Acta Part B* 53 (1998) 1–42.
- [3] F.L. King, W.W. Harrison, Glow discharge mass spectrometry: An introduction to the technique and its utility, *Mass Spec. Rev.* 9 (1990) 285–317.
- [4] A. Bogaerts, R. Gijbels, R.J. Carman, Collisional-radiative model for the sputtered copper atoms and ions in a direct current argon glow discharge, *Spectrochim. Acta Part B* 53 (1998) 1679–1703.
- [5] A. Bogaerts, R. Gijbels, J. Vlcek, Modelling of glow discharge optical emission spectrometry: calculation of the argon atomic optical emission spectrum, *Spectrochim. Acta Part B* 53 (1998) 1517–1526.
- [6] A. Bogaerts, R.D. Guenard, B.W. Smith, J.D. Winefordner, W.W. Harrison, R. Gijbels, Three-dimensional density profiles of argon metastable atoms in direct current glow discharge: experimental study and comparison with calculations, *Spectrochim. Acta Part B* 52 (1997) 219–229.
- [7] A. Bogaerts, R. Gijbels, Modeling of glow discharge sources with flat and pin cathodes and implications for mass spectrometric analysis, *J. Am. Soc. Mass Spectrom.* 8 (1997) 1021–1029.
- [8] A. Bengtson, Developments in glow discharge optical emission spectrometry, *J. Anal. Atom. Spectrom.* 11 (1996) 829–833.
- [9] C.L. Chakrabarti, K.L. Headrick, J.C. Hutton, Z. Bicheng, P.C. Bertels, M.H. Back, Pulsed and transient modes of atomization by cathodic sputtering in a glow discharge for atomic absorption spectrometry, *Anal. Chem.* 62 (1990) 574–586.
- [10] A.E. Bernhard, *Spectroscopy* 2 (1987) 24.
- [11] W. Hang, W.O. Walden, W.W. Harrison, Microsecond pulsed glow discharge as an analytical spectroscopic source, *Anal. Chem.* 68 (1996) 1148–1152.
- [12] C. Yang, K. Ingeneri, W.W. Harrison, A pulsed Grimm glow discharge as an atomic emission source, *J. Anal. At. Spectrom.* 14 (1999) 693–698.
- [13] E. Cordos, H.V. Malmstadt, Characteristics of hollow cathode lamps operated in an intermittent high current mode, *Anal. Chem.* 45 (1973) 27–32.
- [14] H. Duncen, H.J. Tiller, J. Meisel, Uber ein verunreinigungsbedingtes nachleuchten bei einer glimmentladung durch Ar-H₂-mischungen, *Spectrochim. Acta Part B* 24 (1969) 632–634.
- [15] L.R.P. Butler, K. Kroger, C.D. West, Emission spectral analysis with the glow discharge source and a resonance detector, *Spectrochim. Acta Part B* 30 (1975) 489–499.
- [16] C. Pan, F.L. King, Direct determination of trace elements in graphite matrices using modulated glow discharge atomic absorption spectrometry, *Appl. Spectrosc.* 47 (1993) 300–304.
- [17] M. Glick, B.W. Smith, J.D. Winefordner, Laser-excited atomic fluorescence in a pulsed hollow-cathode glow discharge, *Anal. Chem.* 62 (1990) 157–161.
- [18] B.W. Smith, N. Omenetto, J.D. Winefordner, Laser-excited atomic fluorescence in a pulsed glow discharge, *Spectrochim. Acta Part B* 39 (1984) 1389–1393.
- [19] C.V. Dijk, B.W. Smith, J.D. Winefordner, Spatial and temporal studies of a glow discharge, *Spectrochim. Acta Part B* 37 (1982) 759–768.
- [20] J.A. Strauss, N.P. Ferreira, H.G.C. Human, An investigation into the role of metastable argon atoms in the afterglow plasma of a low pressure discharge, *Spectrochim. Acta Part B* 37 (1982) 947–954.
- [21] F.L. King, C. Pan, Temporal signal profiles of analytical species in modulated glow discharge plasmas, *Anal. Chem.* 65 (1993) 735–739.
- [22] A. Walsh, Atomic absorption methods for the direct analysis of metals and alloys, *Appl. Spec.* 27 (1973) 335–341.
- [23] N.P. Ferreira, J.A. Strauss, H.G.C. Human, Distribution of metastable argon atoms in the modified Grimm-type electrical discharge, *Spectrochim. Acta Part B* 37 (1982) 273–279.
- [24] T. Fujimoto, Kinetics of ionization-recombination of plasma and population density of excited ions. I. Equilibrium plasma, *J. Phys. Soc. Jpn.* 47 (1979) 265–272.
- [25] T. Fujimoto, Kinetics of ionization-recombination of plasma and population density of excited ions. IV. Recombining plasma — low temperature case, *J. Phys. Soc. Jpn.* 49 (1980) 1569–1576.
- [26] C. Pan, F.L. King, Time-resolved studies of ionized sputtered atoms in pulsed radio frequency powered glow discharge mass spectrometry, *Anal. Chem.* 65 (1993) 3187–3193.
- [27] C. Pan, F.L. King, Ion formation processes in the after-peak time regime of pulsed glow discharge plasmas, *J. Am. Soc. Mass Spectrom.* 4 (1993) 727–732.
- [28] J.A. Klinger, C.M. Barshick, W.W. Harrison, Factors influencing ion signal profiles in pulsed glow discharge mass spectrometry, *Anal. Chem.* 63 (1991) 2571–2576.
- [29] C.L. Lewis, E.S. Oxley, C.K. Pan, R.E. Steiner, F.L. King, Determination of ⁴⁰Ca⁺ in the presence of ⁴⁰Ar⁺: An illustration of the utility of time-gated detection in pulsed glow discharge mass spectrometry, *Anal. Chem.* 71 (1999) 230–234.
- [30] M. Bourene, J.L. Calve, De-excitation cross sections of metastable argon by various atoms and molecules, *J. Chem. Phys.* 58 (1973) 1452–1458.

- [31] L.G. Piper, J.E. Velazco, D.W. Setser, Quenching cross sections for electronic energy transfer reactions between metastable argon atoms and noble gases and small molecules, *J. Chem. Phys.* 59 (1973) 3323–3340.
- [32] R.E. Steiner, C.L. Lewis, V. Majidi, Consideration of a millisecond pulsed glow discharge time-of-flight mass spectrometer for concurrent elemental and molecular analysis, *J. Anal. At. Spectrom.* 14 (1999) 1537–1541.
- [33] V. Majidi, M. Moser, C. Lewis, W. Hang, F.L. King, Explicit chemical speciation by microsecond pulsed glow discharge time-of-flight mass spectrometry: concurrent acquisition of structural, molecular and elemental information, *J. Anal. At. Spectrom.* 15 (2000) 19–25.
- [34] J.W. Coburn, E. Kay, Plasma diagnostics of an rf-sputtered glow discharge, *Appl. Phys. Lett.* 18 (1971) 435–438.
- [35] R.L. Smith, D. Serxner, K.R. Hess, Assessment of the relative role of Penning ionization in low-pressure glow discharges, *Anal. Chem.* 61 (1989) 1103–1108.
- [36] K.R. Hess, W.W. Harrison, The role of metastable atoms in glow discharge ionization processes, *Anal. Chem.* 60 (1988) 691–696.
- [37] K. Imura, R. Midorikawa, T. Kasai, H. Ohoyama, D. Che, Observation of relative population change in the 3P_0 and 3P_2 states for Ar glow discharge formation, *Chem. Lett.* (1996) 299–300.
- [38] J.E. Velazco, J.H. Kolts, D.W. Setser, Rate constants and quenching mechanisms for the metastable states of argon, krypton, and xenon, *J. Chem. Phys.* 69 (1978) 4357–4373.
- [39] G.H. Copley, C.S. Lee, Electron excitation and deexcitation coefficients for the 3P_2 , 3P_1 , 3P_0 , 1P_1 levels of argon, *Can. J. Phys.* 53 (1975) 1705–1714.
- [40] C.M. Ferreira, J. Loureiro, A. Ricard, Populations in the metastable and resonance levels of argon and stepwise ionization effects in a low-pressure argon positive column, *J. Appl. Phys.* 57 (1985) 82–90.
- [41] K. Hoppstock, W.W. Harrison, Spatial distribution of atoms in a dc glow discharge, *Anal. Chem.* 67 (1995) 3167–3171.
- [42] A. Bogaerts, R. Gijbels, Description of the argon-excited levels in a radio-frequency and direct current glow discharge, *Spectrochim. Acta Part B* 55 (2000) 263–278.
- [43] C.L. Lewis, G.P. Jackson, S.K. Doorn, V. Majidi, F.L. King, Spectral, spatial and temporal characterization of a millisecond-pulsed glow discharge: copper analyte emission and ionization, *Spectrochim. Acta Part B* 56 (2001) 487–501.
- [44] W.L. Wiese, J.W. Brault, K. Danzmann, V. Helbig, M. Kock, Unified set of atomic transition probabilities for argon, *Phys. Rev. A* 39 (1989) 2461–2471.
- [45] P.A. Jansson, *Deconvolution: With Applications in Spectroscopy*, Academic Press, Inc, Orlando FL, 1984.